Gold nanorod photoluminescence : applications to imaging and temperature sensing

Carattino, A.

4

GOLD NANORODS AS NANO-THERMOMETERS

Nano-thermometry is a challenging field that can open the door to very intriguing results ranging from biology and medicine to material sciences. Gold nanorods are excellent candidates to act as nanoprobes because they are reasonably bright emitters upon excitation with a monochromatic source. Moreover gold nanoparticles are already used in photothermal therapy as efficient transducers of electromagnetic radiation into heat. In this work we show that the spectrum of the anti-Stokes emission from gold nanorods irradiated in resonance can be used to measure the absolute temperature of the nanoparticles. The procedure does not require any previous calibration and can be easily implemented in any microscope capable of acquiring emission spectra. We show that the luminescence spectrum of single gold nanorods closely follows Bose-Einstein statistics. We model the emission considering interactions of the electrons and holes created upon absorption of a photon with thermal excitations in the metal, in particular phonons.

4.1. INTRODUCTION

MOST physical, chemical and biological processes depend on temperature. Together with the miniaturization of devices and the advent of nanotechnology the need for measuring temperature with high spatial accuracy started to emerge. Notably in biology[1, 2] and medicine[3] measuring and controlling temperature at a single cell level will provide not only insight into intracellular processes but it will also contribute to a better understanding of the mechanisms involved in proposed new therapies such as photothermal tumor ablation[4] or controlled drug delivery[5, 6].

Probes with distinctive spectral features are ideal candidates for temperature measurements since they provide high spatial accuracy while far-field optics allow a non-contact readout. Some of the proposed strategies include structures that undergo a conformational change upon an increase in temperature[7], thus inducing variations in fluorescence intensity of a dye molecule embedded into them. Also cleverly designed fluorescent probes[8] in which the ratio of particular emission peaks depends on temperature allow a high accuracy and can be used for intracellular thermometry.

The use of anti-Stokes fluorescence emission from lanthanide ions has been studied for several years[9] and can be used to determine temperature with high accuracy. However organic dyes show a very low amount of emitted photons with a higher energy than the excitation energy, rendering their use in biological conditions very challenging. Recently Surface Enhanced Raman Spectroscopy (SERS) allowed to measure changes induced by temperature down to single molecules[10], but a careful calibration of the measurements is crucial.

At a cellular level measuring temperature has been subject to extensive debate[1, 11]. Many cellular processes may be subject to temperature variations, including heat generation at mitochondria. However the measured temperature changes[1] are in the order of 10^5 times higher than the expected values drawn from theoretical models[12]. Moreover new applications in photothermal therapy require locally increasing the temperature in order to induce the death of specific cells in a tissue[5, 13]. Many of these methods employ metallic nanoparticles as heat sources[4, 14] but rely on models[15] or on ad-hoc calibrations to estimate the temperatures reached[16]. Therefore a method that allows both to increase the local temperature and to monitor it will be of great interest in a broad range of fields.

Gold nanoparticles continue to receive a great amount of attention because of their unique optical properties[17]. The collective oscillation of conduction electrons, also known as plasmon, shows a resonance in the visible to near infra-red wavelengths. This resonance can be tuned by changing the shape of the particles[18] and will be responsible for a large absorption and scattering cross section at the resonance wavelength. It is therefore simple to detect nanoparticles in a dark field scattering[19] configuration or via photothermal imaging[20]. Detecting the particles through their luminescence[21] is also possible; their low quantum yield[22–25], in the order of 10^{-5} is compensated by the enhanced cross section. Moreover the luminescence signal is stable over time; gold nanoparticles do not blink nor bleach, therefore are useful labelling agents for processes that require extended periods of observation[26].

Different metallic nano-objects are being introduced as agents for photothermal therapy or drug delivery[5, 13, 27]. One of the advantages of gold nanoparticles is the

possibility of tuning their resonance to the near infra-red range, where the penetration of light into tissues can be of several centimeters[3–5, 13, 14, 28]. Moreover the particles can be used not only for treatment, but also for imaging[5, 15]. In this work we propose that the anti-Stokes luminescence of gold nanorods and nanospheres can be used to measure their temperature with relatively high accuracy.

Luminescence of metallic nanoparticles has been the object of extensive study in recent years. Since the first observation of luminescence from bulk gold[29], different groups have tried to quantitatively describe the observed properties[30, 31], such as the quantum yield[22–25, 32] and the emission spectrum[33]. The cross section of different geometries can be calculated employing different computer packages[34–36], obtaining a vary good agreement between calculations and what is experimentally achievable.

Luminescence from single gold nanoparticles can be observed when irradiating them with a monochromatic source. Gold nanorods present two distinct resonance energies, namely the transverse and the longitudinal plasmon resonance. These particles can therefore be excited efficiently at one of those energies; the transverse resonance corresponds to a wavelength of 532 nm and will give rise to a broad emission with a peak at the longitudinal plasmon energy. Conversely it is possible to excite the particles with a wavelength matching the longitudinal plasmon resonance. In this case the excitation benefits from an enhanced absorption cross section, but the emission that overlaps the plasmon resonance will be mostly blocked by the filters needed to prevent direct excitation light from reaching the detectors.

In this work luminescence refers to the emission from nanoparticles observed at energies different from the excitation energy. Normally it is expected that after absorption of a photon, the electrons in the particle will relax and the emitted photon will appear at lower energies than the excitation. If this is the case, the emission is called Stokes-shifted; however gold nanoparticles when excited in resonance also present a significant emission at higher energies called anti-Stokes emission[37–39].

The mechanism we propose to explain the luminescence from gold nanoparticles is based on the radiative recombination of electrons and holes that are created upon the absorption of an incident photon[29, 32]. The emission will be enhanced by the presence of the surface plasmon acting as an antenna[30]. At the same time, the probability of the interaction of the electron or hole with a thermal bath (a phonon or a carrier) before recombining can give rise to an emitted photon with a higher energy than the excitation photon's[40–42].

A monochromatic photon with energy $\hbar\omega_{\mathrm{L}}$ incident on the particle will give rise to a collective oscillation of the gas of conduction electrons called plasmon. The lifetime of the oscillation can be measured in pulsed experiments or calculated from the inverse of the linewidth and is in the order of 10 fs[43]. The plasmon decays by forming a pair of hot electron and hole with an internal energy equal to the plasmon energy[44–46].

The hot electron and hole cool down by exchanging energy with the lattice on a timescale of $\tau \approx 1$ ps[47]. Before this happens, electron and hole have a small probability of recombining radiatively, i.e. of re-emitting their high electronic energy as a photoluminescence photon. If they have interacted only with static surfaces, their energy will be the same and therefore the emitted photon will have the same energy as the incoming photon, and will not contribute to the measured photoluminescence (as it will be blocked by the

notch filter.) If, on the other hand, they have interacted with a phonon or a thermally excited electron or hole, they may have lost or acquired energy before recombining.

Electron and hole can interact with baths upon recombination, either by creation or annihilaton of a phonon. In both cases the energy available upon recombination cannot much exceed $\hbar\omega_L + k_B T$. It has to be noted that in the hypothesis of a single-photon absorption at low excitation power, the temperature T is that of the baths before absorption, i.e. the temperature of the medium surrounding the particle. This is different from pulsed experiments, in which the electron gas temperature can be orders of magnitude higher than room temperature[48].

Radiative recombination gives rise to weakly emitting sources spectrally and spatially distributed throughout the particle over a broad frequency band with an exponential cutoff at $\hbar\omega_{\mathrm{L}} + k_{\mathrm{B}} T$. The weak recombination emission can be greatly enhanced by the surface plasmon resonance, acting as an antenna. With this model the following predictions can be made. Firstly the emission spectrum must follow the plasmon spectrum if the excitation laser is well above the plasmon resonance as shown in Figure 4.1 in the results. If the excitation falls within the plasmon resonance, the spectrum is expected to follow the plasmon spectrum multiplied by a Bose-Einstein statistics factor arising from phonon population. This factor should be proportional to $\bar{n}$ for anti-Stokes and $\bar{n}+1$ for Stokes processes, where

$$\bar{n} = \left(\exp\frac{\hbar\omega}{k_B T} - 1\right)^{-1}. \tag{4.1}$$

With this model, it can also be predicted that the emission should be polarized; for the longitudinal plasmon of gold nanorods this polarization coincides with the longitudinal axis of the particle[37]. Moreover, the lifetime should be determined by the lifetime of hot electrons and holes and should be significantly shorter than the thermalization time of the carriers. If this was not the case, some interactions would be enough to reduce the carriers' energy and therefore the electron and hole wouldn't have enough energy to produce an optical photon. Finally, only the presence of hot carriers is required in the model. As the wavevectors are randomly distributed at all times, the recombination probability remains constant at all stages of relaxation. Therefore excitation well above the plasmon resonance should excite the photoluminescence with nearly the same efficiency as just above the plasmon resonance[25]. Differences in the distribution of electrons and holes appear if the excitation energy allows interband transitions[44, 49].

In this work we propose to use the anti-Stokes luminescence emission from gold nanoparticles to determine their temperature. According to the model just described, the anti-Stokes emission follows the following form,

$$I(\omega) = \mathrm{I}_{\mathrm{SPR}}(\omega) \cdot \left(\exp\frac{\hbar(\omega-\omega_{\mathrm{L}})}{k_{\mathrm{B}} T} - 1\right)^{-1} \tag{4.2}$$

where I is the intensity, ω is the angular frequency of the photons, ω_{L} is the frequency of the laser, $\hbar$ is Planck's constant, k_{B} the Boltzmann constant. $\mathrm{I}_{\mathrm{SPR}}$ is the surface plasmon resonance that can be obtained by exciting the particle at energies higher than the resonance or, ideally, by looking at the scattering spectrum. Even if these two spectra are not identical, they overlap in the range of wavelengths comprising the maximum of the

emission and longer[24]; in the results section a lengthier discussion will be given. The only remaining free parameter is the temperature T (plus a normalization constant not included in eqn. 4.2.) This means that carefully fitting the emission spectra excited at two frequencies ($\nu \gg \nu_{SPR}$ and $\nu \approx \nu_{SPR}$) allows us to extract the absolute temperature of the particles without any previous calibration.

4.2. EXPERIMENTAL METHOD

All the measurements in this work were performed with a home-built confocal microscope equipped with an APD and a spectrometer (Acton 500i). Samples were mounted in a flow cell that allowed us to increase the temperature of the medium up to $60\,^oC$ and to monitor it through a Pt100 resistance thermometer placed 1 mm away from the observation area.

Samples were prepared by spin casting a suspension of nanoparticles onto clean coverslips. Different particles were employed in this work. Nanorods with average dimensions of 21 nm × 50 nm and a plasmon resonance around 650 nm were synthesized following the seeded-growth method[50]; spheres with radii between 30 nm and 60 nm were purchased from BBI International. We employed a 532 nm (CNI) laser for characterizing the nanorods' plasmon and for exciting spheres close to resonance. A 633 nm HeNe (Thorlabs) was employed to excite the nanorods in resonance.

Room temperature measurements were performed using a $60X$, NA 1.4 oil immersion objective (Olympus). This provided high excitation and collection efficiency. At higher temperatures an air-spaced objective, $60X$, NA 0.9 (Olympus) was employed to avoid the presence of a heat sink directly in contact to the observed area. With this objective both the excitation and collection efficiencies are significantly lower. The lower excitation efficiency can be compensated increasing the excitation power, the lower collection however is inherent to the method and can be compensated only by increasing the exposure time.

To compensate for the drift of the setup while increasing the temperature, we developed a computer program to continuously track a reference particle. The same program was responsible for recording the temperature and triggering the spectrometer. In this way complete data sets were acquired at different temperatures, including spectra while exciting at 532 nm, at 633 nm with different laser intensities and the temperature measured by the Pt100. A spectrum with 532 nm laser excitation was taken after every cycle to ensure that the particle was not reshaping due to higher excitation powers.

The intensity of the lasers was controlled via the voltage applied to an AOM in the optical path. Several accumulations of the spectra at the same laser intensity were recorded. This not only allowed us to lower the noise of the measurements because of a longer exposure time, but also allowed us to remove bright pixels generated by cosmic rays. Having several accumulations is also useful to monitor changes in the intensity of the spectra during the acquisition itself. These changes can be due to a drift of the setup while measuring or to a reshaping of the particle. The reshaping can be confirmed by comparing the spectra acquired with the 532 nm laser[51]. In case reshaping was observed, the measurements where rejected. In the case of drift of the setup, the particular data set was not taken into account. For the purposes of this work the excitation intensity is crucial for characterizing the method; if the particle is not in focus it would result in an over estimation of the excitation power.

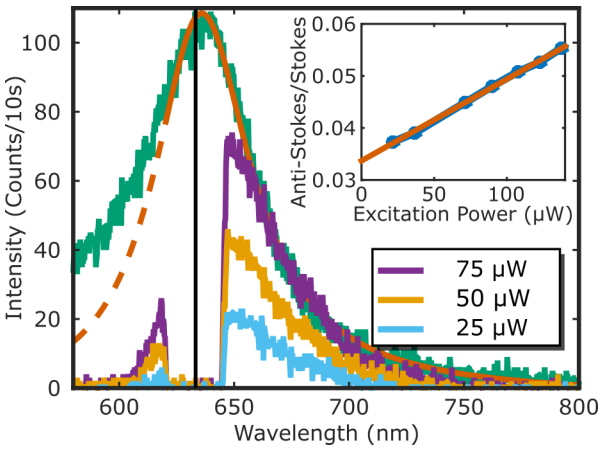

Figure 4.1: Luminescence spectra of a single gold nanorod. The green curve is the emission under 532 nm excitation. In red is the fitting by a lorentzian; the dashed part is the region that was not considered for the fitting. The other curves are the emission of the same particle under 633 nm irradiation at three different powers. The inset shows the anti-Stokes-to-Stokes ratio as a function of the excitation power, overlapped with a linear fit in red.

To calculate the heating of the particles the absorption cross section has to be computed. For the case of nanorods, the ADDA package was employed[34]. Spheres' cross section can be calculated from Mie theory. Once the dissipated power is known, the parameters can be either used in a Comsol model or the heat equation can be analytically solved, approximating the rods by spheres with the same total area.

4.3. RESULTS

The proposed model for the anti-Stokes emission requires to know the plasmon spectrum (I_{SPR} function in equation 4.2) of the particle in order to fit the emission at shorter wavelengths and extract the particle temperature. It has been shown that both scattering and luminescence spectra roughly overlap over a broad range of wavelengths[24]. Therefore exciting gold nanorods with 532 nm allows to record the longitudinal plasmon spectra, as shown in the green solid curve of Figure 4.1. The peak was fitted by a single lorentzian, shown in red in the Figure; the dashed part of the curve depicts the spectral region that was not considered for the fitting. It has to be recalled that the luminescence spectrum is not a perfect lorentzian since there is a broadband contribution to the luminescence arising between the excitation wavelength and the plasmon peak[52]. This appears as an asymmetry in the emission spectrum, particularly visible for wavelengths smaller than 625 nm. The results of this fitting will be employed for the I_{SPR} function defined in equation 4.2.

The other curves in Fig. 4.1 show the luminescence emission of the same nanorod while irradiating with a 633 nm laser at different powers, ranging from 25 μW to 75 μW at the back aperture of the objective. The vertical black line shows the wavelength of the laser. The Stokes part of the spectrum at longer wavelengths than the excitation

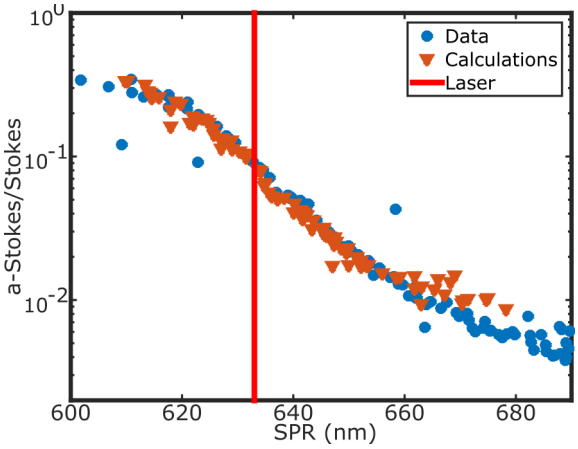

Figure 4.2: Ratio of the anti-Stokes to Stokes emission under 633 nm excitation as function of the resonance wavelength of each particle. The blue circles are experimental results, while the red triangles are the results of the calculations with equation 1.2. There is a very good agreement between experiment and calculations. Particles with a resonance to the blue of the laser (vertical red line) have an increased anti-Stokes emission.

shows the same shape as the plasmon emission observed under 532 nm excitation, apart from a normalization factor. From the figure it can readily be seen that the shape of the anti-Stokes emission, at shorter wavelengths than excitation, is exponential-like and doesn't follow the lorentzian shape of the Stokes emission. The dip between Stokes and anti-Stokes is caused by the notch filter that prevents direct excitation light from reaching the detectors.

The inset of Fig. 4.1 shows the anti-Stokes-to-Stokes ratio of the integrated luminescence for different laser excitation intensities. It is possible to see that even with a linear behavior, the anti-Stokes intensity increases more rapidly with laser excitation power than the Stokes emission. We already exploited this phenomenon to image gold nanorods in high-background conditions[39]. Moreover it shows that the anti-Stokes emission depends on laser excitation power differently from its Stokes counterpart.

Figure C.2 shows the intensity of the Stokes (red) and anti-Stokes (blue) emission for several excitation powers. In both cases the linear fit in logarithmic scale has a slope close to 1, being 0.88 for the Stokes and 1.20 for the anti-Stokes, confirming that both types of emission are single-photon processes. The behavior is independent of the plasmon resonance position. It is important to note that the excitation intensity cannot be increased much beyond what is shown because nanorods would start reshaping towards a more spherical shape at higher laser powers.

Figure 4.2 shows the ratio of the anti-Stokes to Stokes emission for 90 nanorods with different plasmon resonances and under 633 nm excitation; the blue circles are experimental data. The horizontal axis of the figure is the surface plasmon resonance (SPR) of each particle. The vertical red line marks the laser wavelength. The particles shown in the plot had resonances between 600 nm and 690 nm; the ones showing the maximum ratio of anti-Stokes to Stokes are those with a resonance to the blue of the laser. For these particles the plasmon is enhancing preferably the anti-Stokes emission. For

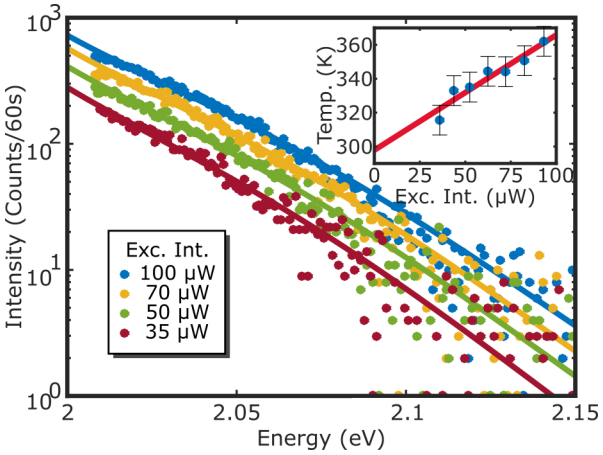

Figure 4.3: Anti-Stokes emission at different irradiation powers with the corresponding fits by equation 4.2. There is an excellent agreement between data and model. The inset shows the extracted temperature at each power (blue dots) and a linear extrapolation of the data to 0 μW excitation power. The value obtained for room temperature was 293 K while the measured value was 296 K.

particles with a resonance at the laser wavelength the anti-Stokes and the Stokes emission have similar enhancement and show a ratio close to 10%.

Figure 4.2 also shows the results of calculations as the red triangles. A very good overlap between the measured and the calculated data can be observed. The absorption cross section of several particles was calculated with the ADDA package. Each calculated absorption spectrum was fitted by a lorentzian and used as $I_{SPR}(\omega)$ in eqn. 4.2. The absorption cross section also allowed us to estimate the temperature of the particle assuming a diffraction limited laser spot and from this to calculate the anti-Stokes emission spectrum using the full eqn. 4.2. The Stokes emission was calculated assuming a lorentzian spectrum overlapping the absorption. Both anti-Stokes and Stokes emissions are proportional to the excitation power, so that this term cancels out when computing the ratio. For this calculation no free parameters were assumed and the transmission of the filters was taken into account.

By fitting the anti-Stokes part of the spectra shown in Fig. 4.1 with equation 4.2 it is possible to extract the temperature of the particle at each excitation power. Figure 4.3 shows the results of this procedure. The spectra shown were recorded at 4 different excitation intensities while the full lines are the fits; there is an excellent agreement between data and model. For every anti-Stokes measurement we have also acquired the full plasmon spectrum while exciting with a 532 nm laser before and after the temperature extraction. Having the full plasmon spectrum allowed us to calculate the parameters of I_{SPR} from equation 4.2 and also to verify that the particle didn't reshape while being excited at resonance.

The inset in fig. 4.3 shows the temperatures resulting from the fits at different irradiation intensities (blue dots). It is remarkable that the absolute temperatures of the particle were extracted without any previous calibration. As expected, the temperature of the nanorod is proportional to the excitation intensity, or equivalently to the absorbed energy.

From these data it is also possible to calculate the temperature at 0 μW excitation power, i.e. room temperature, by extrapolating the results of a linear fit. The value we obtained in this case is 293 ± 6 K, while room temperature was 296 K, a 2% accuracy.

The accuracy of the obtained temperature depends to a great extent on the plasmon resonance. The first step in the fitting of spectra is the determination of the term I_{SPR} in equation 4.2. This is achieved by fitting a lorentzian to the emission spectrum obtained while irradiating with a 532 nm laser. In figure 4.1 it is possible to observe that the emission spectrum is not perfectly lorentzian and therefore the fitting results will be sensitive to the portion of the spectrum selected. Depending on the wavelength range selected, the parameters of the lorentzian fit (its width and peak position) can slightly change and this will give rise to different temperatures when fitting the anti-Stokes emission spectrum.

Equation 4.2 shows that if the particle plasmon resonance is red shifted with respect to the 633 nm laser, the term I_{SPR} will have a smaller effect on the temperature extracted. When the resonance is to the red of the laser, the term I_{SPR} will slowly vary in the region where the anti-Stokes emission is observed. Therefore small changes in the parameters of the lorentzian fit will have a small effect on the temperature extracted. However, particles that are not in resonance with the excitation laser will present a lower emission due to a smaller absorption cross section and to a lower enhancement of the anti-Stokes emission (see for example figure 4.2). A balance between the amount of collected light and the uncertainty produced by the correct determination of the plasmon resonance has to be reached depending on each application. The error bar in figure 4.3 and in the following figures is the result of the estimation of the temperature uncertainty because of variations in the plasmon resonance fit.

As expected from the model, the anti-Stokes emission should depend not only on the particle's intrinsic properties but also on the temperature of the surrounding medium[53]. The samples were therefore mounted in a flow cell that allowed us to change the temperature and to measure it with a Pt100 resistance thermometer. In this set of experiments we employed a dry objective and therefore the laser powers are higher to compensate for the lower excitation efficiency. At each temperature several spectra were acquired at different 633 nm excitation powers and also a spectrum of the plasmon before and after each measurement in order to monitor any possible reshaping of the particles during the experiment.

Figure 4.4 shows the extracted temperature of a particle at varying excitation powers and at different water temperatures. The blue circles are the results of the measurement at 20 ^{o}C, while the green crosses are at 40 ^{o}C and the yellow squares at 60 ^{o}C. The full lines are the calculated temperatures for a particle with plasmon overlapping the measured one and assuming a diffraction-limited focus spot. For the dimensions of the particle, the mean values from TEM images were used and the length was adjusted to obtain the same resonance. There is a remarkable agreement between the calculation and the measured values. Moreover it is possible to extrapolate the temperature at zero excitation power for each case as was explained earlier. The results are shown in the inset of the figure for each temperature. The red line with slope 1 is a guide to the eye.

Figure 4.4 clearly shows that the extracted temperature varies with the temperature of the surrounding medium. More strikingly the method does not require any previous calibration nor adjustment. The values obtained with the extrapolation to 0 μW excitation

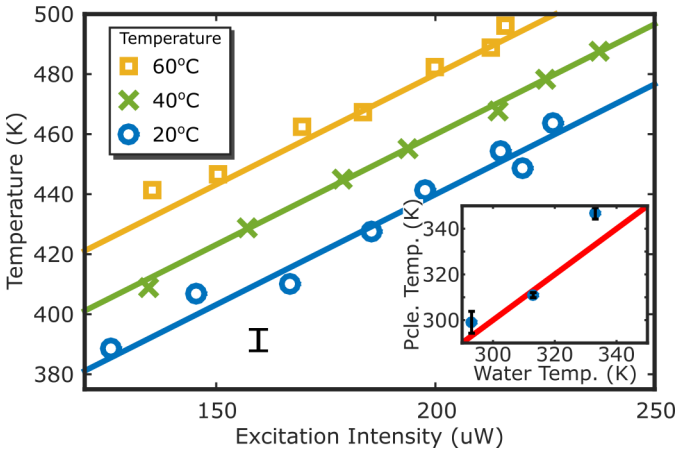

Figure 4.4: Extracted temperatures at different excitation powers and at different flow cell temperatures. The full lines are the results of the calculated temperatures. The inset shows the extrapolated temperature at zero excitation power.

power were 299 ± 8 K, 311 ± 3 K and 347 ± 6 K for water temperatures of 293 K, 313 K and 333 K respectively. The very good agreement between the temperatures obtained from fitting the anti-Stokes emission and the water temperatures measured by the Pt100 thermometer is remarkable. The calibration-free procedure would allow us to perform the same measurements in any other setup and could act as a reference for calibration of other nano thermometers.

It is also possible to keep the excitation intensity constant and to vary the temperature of the surrounding medium. Figure 4.5 shows the extracted temperature from the fitting with equation 4.2 as a function of the temperature of the medium. The red line is showing the water temperature and acts as a guide to the eye. The Figure clearly shows an increase in the extracted temperature while increasing the temperature of the flow cell. The range of explored temperatures was from 296 K to 320 K. This range is enough to observe a change in the anti-Stokes emission spectrum. At higher temperatures the stability of the setup plays a crucial role in maintaining the particle in focus during the spectra acquisition time. Longer exposure times and therefore lower excitation intensities can be employed if particles are actively maintained in focus.

Particles that can withstand higher excitation powers and that have a well-defined plasmon resonance are of great interest, because they would allow to employ a single wavelength and also to reduce the exposure times to record the spectra. A well defined plasmon resonance also lowers the uncertainties associated with the initial lorentzian fit needed for the term I_{SPR} in equation 4.2. In principle gold nanospheres fulfill these requirements. They are known to withstand much higher excitation powers without reshaping nor melting[54]. Moreover the plasmon resonance of spheres shifts only slightly with radius, therefore it is possible to predict it using Mie theory and to eliminate the need of a second laser beam. Sphere samples however always show a shape distribution that cannot be neglected[55] and that induces deviations of the observed resonance from

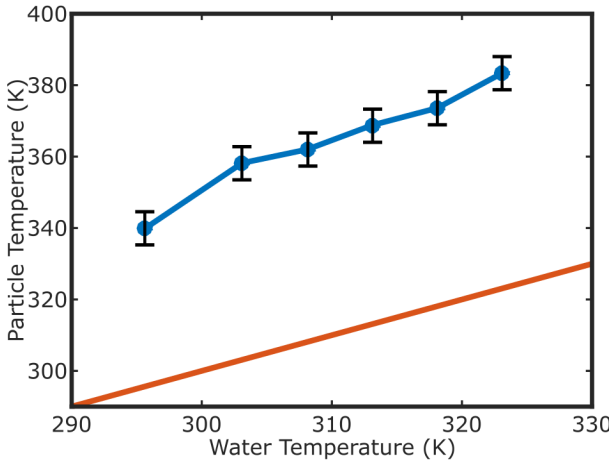

Figure 4.5: Temperature of a single nanorod under the same 633 nm excitation conditions, but at different medium temperatures.

Mie's model.

Figure 4.6 shows the normalized luminescence spectra of three nanospheres of diameters 60 nm, 40 nm and 30 nm under 532 nm excitation. As for the nanorods, two very distinctive parts of the spectrum are distinguishable, the Stokes spectrum at longer wavelengths and the anti-Stokes spectrum at shorter ones. From Mie theory we would have expected a blue shift of the resonance whith decreasing radius of the particles; however the 30 nm sphere seems to be the most red-shifted. This is most likely due to small anisotropies of the particles, giving rise to slightly different plasmon resonances. The inset in Fig.4.6 shows a detail of the anti-Stokes emission for the three spheres without any further normalization. It has to be pointed out, however, that the excitation intensities were 1.2 mW, 2.0 mW and 3.6 mW to compensate for the lower cross sections of the smaller particles.

Spheres not only have a smaller cross section than nanorods of the same volume, but their quantum yield is also one order of magnitude lower than that of rods[24]. The weaker emission from these particles can be compensated by increasing the excitation power. The maximum power that can be employed is given by either reaching the melting temperature of gold or by inducing a phase transition of the surrounding liquid. The first would induce an irreversible change in shape of the particles[56] the latter would induce a change in the refractive index of the medium and therefore would induce a shift in the plasmon resonance[54].

Figure 4.7 shows the extracted temperature of the three particles while increasing the medium temperature. It is possible to see that the small 30 nm diameter sphere is 150 K hotter than both the 40 nm and 60 nm. The three curves show an increasing trend, but in this case the variation of medium temperature amounts to less than 5% the temperature of the particles. The extracted temperature is several tens of degrees above what would be expected from the heat equation, considering the absorption cross section given by Mie theory. The reason for the discrepancies between the measured values and the expected

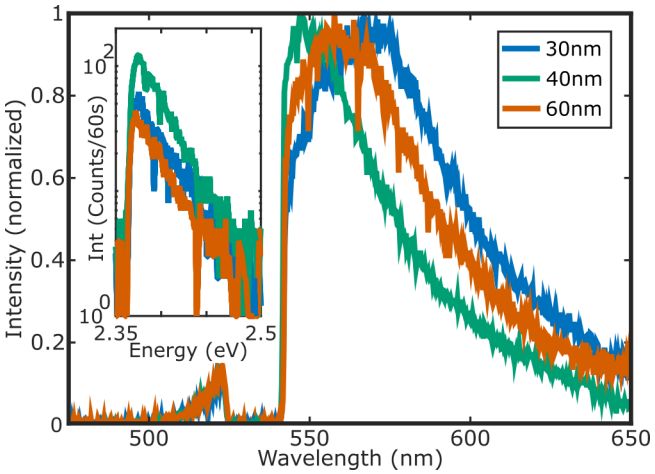

Figure 4.6: Normalized luminescence spectra of spheres with diameters of 60 nm, 40 nm and 30 nm under 532 nm excitation. The inset shows the detail of the anti-Stokes emission without normalization. The excitation powers for the three particles were 1.2 mW, 2.0 mW and 3.6 mW respectively.

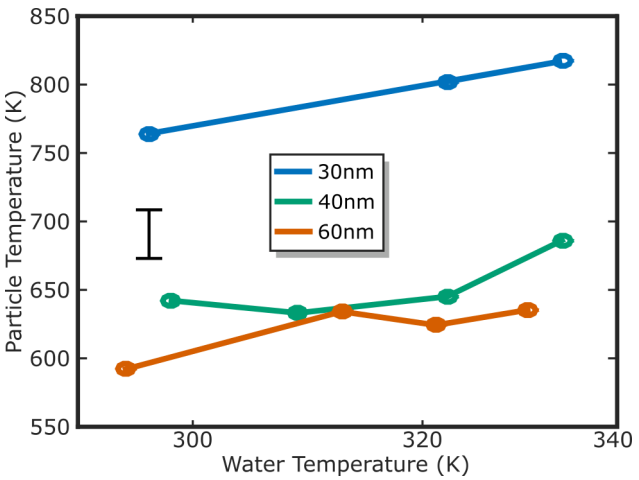

Figure 4.7: Extracted temperature from the same particles as in fig. 4.6 at different medium temperatures.

values can be accounted for by the computation of the plasmon resonance term I_{SPR} in eqn. 4.2.

As explained earlier for nanorods, the fitting of the anti-Stokes emission is highly sensitive to the plasmon position relative to the laser employed. In the case of nanospheres, the resonance is slightly shifted to the red from the 532 nm laser. Small errors in the determination of the plasmon resonance will generate larger errors in the temperature extracted. The differences between the plasmon observed in fig. 4.6 and the results of Mie scattering calculations most likely are due to particles that are not spherical. If this was the case, the calculated cross section and plasmon resonance will not coincide with the particles under study, leading to larger errors.

The use of spheres would be beneficial for some applications that require higher excitation powers or smaller particles. The intrinsic heterogeneity of the samples, however, prevents the use of a single wavelength for the measurements. Ideally, white light scattering of single gold nanospheres would provide the information on the plasmon resonance needed for the correct fitting of the anti-Stokes emission.

4.4. CONCLUSIONS

Being able to control and monitor temperature at the nanoscale is of utmost importance in different fields ranging from photothermal therapy[5] to nano fabrication[57]. In this work we have shown a simple procedure that allows us to measure the temperature of single gold nanorods and nanospheres irradiated under a monochromatic continuous laser and without any previous calibration. The level of accuracy of the temperature measurement depends on several factors, but for nanorods it can be estimated to be better than 6 K and for nanospheres around 15 K.

The model employed for describing the anti-Stokes emission takes into account the plasmon, responsible for enhancing the emission, as well as Bose-Einstein statistics to explain the distribution of the excited states of the particles. It has been shown that the correct characterization of the plasmonic resonance is fundamental for the proper extraction of temperature, specially in cases where the excitation wavelength is red-detuned from the resonance.

Particles with a resonance to the red of the excitation wavelength would be more reliable in the temperature extraction procedure, but would also exhibit a lower emission towards shorter wavelengths. The trade-off between both effects and the possibility to fully characterize the plasmon resonance, will determine the specific particles that are better suited for each application.

In this work we have also explored the possibility of employing gold nanospheres. Since these particles do not reshape under higher excitation powers it is possible to compensate their lower cross section by increasing the irradiation intensity. However, their quantum yield is at least one order of magnitude smaller than that of rods, giving an overall lower photoluminescence intensity. Samples with a narrow shape distribution such as bipyramids[58] would be ideal candidates to temperature extraction since their plasmon can be measured or determined from theory, avoiding the need of a second excitation source.

We have observed the anti-Stokes emission from particles with three different diameters. It was already possible to see that the heterogeneity in the shape of the particles

induces plasmon resonances different from the ones predicted from Mie theory. The variation in the temperature extracted from the anti-Stokes spectra while increasing the medium's temperature falls within the experimental error. The obtained temperatures however are much higher than predicted from the heat equation. The samples normally have a distribution of sizes and shapes, assuming a perfectly spherical particle leads to an incorrect determination of the plasmon resonance that propagates into the determination of the surface temperature.

The main advantage of the proposed method is that it doesn't require any calibration, since the only free parameter of the model is the absolute temperature of the nanoparticle under study. Moreover the recording of the anti-Stokes spectrum is readily achievable in any confocal microscope with a coupled spectrometer. A 6 K accuracy may suffice for several applications; it is important to point out that this value can be improved in different ways: by carefully selecting the particles that show the most favorable plasmon resonance; by determining the plasmon resonance through white-light scattering, avoiding the uncertainty in the fit; by increasing the exposure times to increase the signal-to-noise ratio; finally an ad-hoc calibration of the temperature can be performed.

REFERENCES

[1] J.-M. Yang, H. Yang, and L. Lin, *Quantum Dot Nano Thermometers Reveal Heterogeneous Local Thermogenesis in Living Cells,* ACS Nano **5**, 5067 (2011).

[2] C. Hrelescu, J. Stehr, M. Ringler, R. A. Sperling, W. J. Parak, T. A. Klar, and J. Feldmann, *DNA Melting in Gold Nanostove Clusters,* J. Phys. Chem. C **114**, 7401 (2010).

[3] Y. Li, A. M. Gobin, G. W. Dryden, X. Kang, D. Xiao, S. P. Li, G. Zhang, and R. C. G. Martin, *Infrared light-absorbing gold/gold sulfide nanoparticles induce cell death in esophageal adenocarcinoma,* Int. J. Nanomedicine **8**, 2153 (2013).

[4] A. M. Gobin, M. H. Lee, N. J. Halas, W. D. James, R. A. Drezek, J. L. West, M. Gobin, M. H. Lee, N. J. Halas, W. D. James, R. A. Drezek, and J. L. West, *Near-Infrared Resonant Nanoshells for Combined Optical Imaging and Photothermal Cancer Therapy,* Nano Lett. **7**, 1929 (2007).

[5] X. H. Huang, I. H. El-Sayed, W. Qian, and M. a. El-Sayed, *Cancer cell imaging and photothermal therapy in the near-infrared region by using gold nanorods,* J. Am. Chem. Soc. **128**, 2115 (2006).

[6] S. Huo, S. Jin, X. Ma, X. Xue, K. Yang, A. Kumar, P. C. Wang, J. Zhang, Z. Hu, and X.-J. Liang, *Ultrasmall Gold Nanoparticles as Carriers for Nucleus-Based Gene Therapy Due to Size-Dependent Nuclear Entry,* ACS Nano **8**, 5852 (2014).

[7] S. Ebrahimi, Y. Akhlaghi, M. Kompany-Zareh, and A. Rinnan, *Nucleic Acid Based Fluorescent Nanothermometers.* ACS Nano (2014), 10.1021/nn5036944.

[8] F. Vetrone, R. Naccache, A. Zamarrón, A. Juarranz de la Fuente, F. Sanz-Rodríguez, L. Martinez Maestro, E. Martín Rodriguez, D. Jaque, J. García Solé, and J. A. Capobianco, *Temperature sensing using fluorescent nanothermometers,* ACS Nano **4**, 3254 (2010), http://dx.doi.org/10.1021/nn100244a .

[9] F. Auzel, *Upconversion and Anti-Stokes Processes with f and d Ions in Solids,* Chem. Rev. **104**, 139 (2004).

[10] E. A. Pozzi, A. B. Zrimsek, C. M. Lethiec, G. C. Schatz, M. C. Hersam, and R. P. Van Duyne, *Evaluating Single-Molecule Stokes and Anti-Stokes SERS for Nanoscale Thermometry,* J. Phys. Chem. C **119**, 21116 (2015).

[11] M. Suzuki, V. Zeeb, S. Arai, K. Oyama, and S. Ishiwata, *The 10^5 gap issue between calculation and measurement in single-cell thermometry,* Nat. Methods **12**, 802 (2015).

[12] M. K. Sato, M. Toda, N. Inomata, H. Maruyama, Y. Okamatsu-Ogura, F. Arai, T. Ono, A. Ishijima, and Y. Inoue, *Temperature Changes in Brown Adipocytes Detected with a Bimaterial Microcantilever,* Biophys. J. **106**, 2458 (2014).

[13] X. Huang, P. K. Jain, I. H. El-Sayed, and M. A. El-Sayed, *Plasmonic photothermal therapy (PPTT) using gold nanoparticles,* Lasers Med. Sci. **23**, 217 (2008).

[14] L. R. Hirsch, R. J. Stafford, J. A. Bankson, S. R. Sershen, B. Rivera, R. E. Price, J. D. Hazle, N. J. Halas, and J. L. West, *Nanoshell-mediated near-infrared thermal therapy of tumors under magnetic resonance guidance.* Proc. Natl. Acad. Sci. U. S. A. **100**, 13549 (2003), arXiv:0008204 [cond-mat] .

[15] T. Zhao, K. Yu, L. Li, T. Zhang, Z. Guan, N. Gao, P. Yuan, S. Li, S. Q. Yao, Q.-H. Xu, and G. Q. Xu, *Gold Nanorod Enhanced Two-Photon Excitation Fluorescence of Photosensitizers for Two-Photon Imaging and Photodynamic Therapy,* ACS Appl. Mater. Interfaces **6**, 2700 (2014).

[16] J. S. Donner, S. a. Thompson, C. Alonso-Ortega, J. Morales, L. G. Rico, S. I. C. O. Santos, and R. Quidant, *Imaging of Plasmonic Heating in a Living Organism,* ACS Nano **7**, 8666 (2013).

[17] P. Zijlstra and M. Orrit, *Single metal nanoparticles: optical detection, spectroscopy and applications,* Reports Prog. Phys. **74**, 106401 (2011).

[18] A. Carattino, S. Khatua, and M. Orrit, *In situ tuning of gold nanorod plasmon through oxidative cyanide etching,* Phys. Chem. Chem. Phys. **18**, 15619 (2016).

[19] M. Hu, C. Novo, A. Funston, H. Wang, H. Staleva, S. Zou, P. Mulvaney, Y. Xia, and G. V. Hartland, *Dark-field microscopy studies of single metal nanoparticles: understanding the factors that influence the linewidth of the localized surface plasmon resonance,* J. Mater. Chem. **18**, 1949 (2008).

[20] S. Berciaud, D. Lasne, G. Blab, L. Cognet, and B. Lounis, *Photothermal heterodyne imaging of individual metallic nanoparticles: Theory versus experiment,* Phys. Rev. B **73**, 045424 (2006).

[21] A. Tcherniak, S. Dominguez-Medina, W.-S. Chang, P. Swanglap, L. S. Slaughter, C. F. Landes, and S. Link, *One-Photon Plasmon Luminescence and Its Application to Correlation Spectroscopy as a Probe for Rotational and Translational Dynamics of Gold Nanorods,* J. Phys. Chem. C **115**, 15938 (2011).

[22] Y. Fang, W.-S. Chang, B. Willingham, P. Swanglap, S. Dominguez-Medina, and S. Link, *Plasmon emission quantum yield of single gold nanorods as a function of aspect ratio.* ACS Nano **6**, 7177 (2012).

[23] W. Rao, Q. Li, Y. Wang, T. Li, and L. Wu, *Comparison of Photoluminescence Quantum Yield of Single Gold Nanobipyramids and Gold Nanorods,* ACS Nano **9**, 2783 (2015).

[24] M. Yorulmaz, S. Khatua, P. Zijlstra, A. Gaiduk, and M. Orrit, *Luminescence quantum yield of single gold nanorods.* Nano Lett. **12**, 4385 (2012).

[25] Y. Cheng, G. Lu, Y. He, H. Shen, J. Zhao, K. Xia, and Q. Gong, *Luminescence Quantum Yields of Gold Nanoparticles Varying with Excitation Wavelength,* Nanoscale , 2188 (2015).

[26] H. Wang, T. B. Huff, D. A. Zweifel, W. He, P. S. Low, A. Wei, and J.-X. Cheng, *In vitro and in vivo two-photon luminescence imaging of single gold nanorods,* Proc. Natl. Acad. Sci. **102**, 15752 (2005).

[27] B. Kang, M. M. Afifi, L. a. Austin, and M. a. El-Sayed, *Exploiting the nanoparticle plasmon effect: observing drug delivery dynamics in single cells via Raman/fluorescence imaging spectroscopy.* ACS Nano **7**, 7420 (2013).

[28] D. O'Neal, L. R. Hirsch, N. J. Halas, J. Payne, and J. L. West, *Photo-thermal tumor ablation in mice using near infrared-absorbing nanoparticles,* Cancer Lett. **209**, 171 (2004).

[29] A. Mooradian, *Photoluminescence of metals,* Phys. Rev. Lett. **22**, 185 (1969).

[30] M. B. Mohamed, V. Volkov, S. Link, and M. A. El-Sayed, *The 'lightning' gold nanorods: fluorescence enhancement of over a million compared to the gold metal,* Chem. Phys. Lett. **317**, 517 (2000).

[31] M. Beversluis, A. Bouhelier, and L. Novotny, *Continuum generation from single gold nanostructures through near-field mediated intraband transitions,* Phys. Rev. B **68**, 1 (2003).

[32] E. Dulkeith, T. Niedereichholz, T. Klar, J. Feldmann, G. von Plessen, D. Gittins, K. Mayya, and F. Caruso, *Plasmon emission in photoexcited gold nanoparticles,* Phys. Rev. B **70**, 205424 (2004).

[33] S. Link and M. A. El-Sayed, *Shape and size dependence of radiative, non-radiative and photothermal properties of gold nanocrystals,* Int. Rev. Phys. Chem. **19**, 409 (2000).

[34] M. A. Yurkin and A. G. Hoekstra, *The discrete-dipole-approximation code ADDA: Capabilities and known limitations,* J. Quant. Spectrosc. Radiat. Transf. **112**, 2234 (2011).

[35] B. T. Draine and P. J. Flatau, *Discrete-Dipole Approximation For Scattering Calculations,* J. Opt. Soc. Am. A **11**, 1491 (1994).

[36] A. F. Oskooi, D. Roundy, M. Ibanescu, P. Bermel, J. Joannopoulos, and S. G. Johnson, *Meep: A flexible free-software package for electromagnetic simulations by the FDTD method,* Comput. Phys. Commun. **181**, 687 (2010).

[37] Y. He, K. Xia, G. Lu, H. Shen, Y. Cheng, Y.-c. Liu, K. Shi, Y.-F. Xiao, and Q. Gong, *Surface enhanced anti-Stokes one-photon luminescence from single gold nanorods,* Nanoscale **7**, 577 (2015).

[38] L. Jiang, I. W. Schie, J. Qian, S. He, and T. Huser, *Coherent Anti-Stokes Emission from Gold Nanorods and its Potential for Imaging Applications,* ChemPhysChem **14**, 1951 (2013).

[39] A. Carattino, V. I. Keizer, M. J. Schaaf, and M. Orrit, *Background Suppression in Imaging Gold Nanorods through Detection of Anti-Stokes Emission,* Biophys. J. **111**, 2492 (2016).

[40] J. H. Hodak, A. Henglein, and G. V. Hartland, *Electron-phonon coupling dynamics in very small (between 2 and 8 nm diameter) Au nanoparticles,* J. Chem. Phys. **112**, 5942 (2000).

[41] A. Giri, J. T. Gaskins, B. M. Foley, R. Cheaito, and P. E. Hopkins, *Experimental evidence of excited electron number density and temperature effects on electron-phonon coupling in gold films,* J. Appl. Phys. **117**, 044305 (2015).

[42] A. Arbouet, C. Voisin, D. Christofilos, P. Langot, N. D. Fatti, F. Vallée, J. Lermé, G. Celep, E. Cottancin, M. Gaudry, M. Pellarin, M. Broyer, M. Maillard, M. P. Pileni, and M. Treguer, *Electron-Phonon Scattering in Metal Clusters,* Phys. Rev. Lett. **90**, 177401 (2003).

[43] C. Sönnichsen, T. Franzl, T. Wilk, G. von Plessen, J. Feldmann, O. Wilson, and P. Mulvaney, *Drastic Reduction of Plasmon Damping in Gold Nanorods,* Phys. Rev. Lett. **88**, 077402 (2002).

[44] R. Sundararaman, P. Narang, A. S. Jermyn, W. a. Goddard III, and H. a. Atwater, *Theoretical predictions for hot-carrier generation from surface plasmon decay,* Nat. Commun. **5**, 5788 (2014).

[45] M. L. Brongersma, N. J. Halas, and P. Nordlander, *Plasmon-induced hot carrier science and technology,* Nat. Nanotechnol. **10**, 25 (2015).

[46] A. Manjavacas, J. G. Liu, V. Kulkarni, and P. Nordlander, *Plasmon-Induced Hot Carriers in Metallic Nanoparticles,* ACS Nano **8**, 7630 (2014).

[47] V. K. Pustovalov, *Theoretical study of heating of spherical nanoparticle in media by short laser pulses,* Chem. Phys. **308**, 103 (2005).

[48] G. Baffou, P. Berto, E. Bermúdez Ureña, R. Quidant, S. Monneret, J. Polleux, and H. Rigneault, *Photoinduced Heating of Nanoparticle Arrays,* ACS Nano **7**, 6478 (2013).

[49] A. M. Brown, R. Sundararaman, P. Narang, W. A. Goddard, and H. A. Atwater, *Ab initio phonon coupling and optical response of hot electrons in plasmonic metals,* Phys. Rev. B **94**, 075120 (2016), arXiv:1602.00625 .

[50] B. Nikoobakht and M. A. El-Sayed, *Preparation and Growth Mechanism of Gold Nanorods (NRs) Using Seed-Mediated Growth Method,* Chem. Mater. **15**, 1957 (2003).

[51] Y. Liu, E. N. Mills, and R. J. Composto, *Tuning optical properties of gold nanorods in polymer films through thermal reshaping,* J. Mater. Chem. **19**, 2704 (2009).

[52] G. T. Boyd, Z. H. Yu, and Y. R. Shen, *Photoinduced luminescence from the noble metals and its enhancement on roughened surfaces,* Phys. Rev. B **33**, 7923 (1986).

[53] A. Konrad, F. Wackenhut, M. Hussels, A. J. Meixner, and M. Brecht, *Temperature Dependent Luminescence and Dephasing of Gold Nanorods,* J. Phys. Chem. C **117**, 21476 (2013).

[54] L. Hou, M. Yorulmaz, N. R. Verhart, and M. Orrit, *Explosive formation and dynamics of vapor nanobubbles around a continuously heated gold nanosphere,* New J. Phys. **17**, 13050 (2015).

[55] Y.-J. Lee, N. B. Schade, L. Sun, J. a. Fan, D. R. Bae, M. M. Mariscal, G. Lee, F. Capasso, S. Sacanna, V. N. Manoharan, and G.-R. Yi, *Ultrasmooth, highly spherical monocrystalline gold particles for precision plasmonics.* ACS Nano **7**, 11064 (2013).

[56] P. Zijlstra, J. W. M. Chon, and M. Gu, *White light scattering spectroscopy and electron microscopy of laser induced melting in single gold nanorods,* Phys. Chem. Chem. Phys. **11**, 5915 (2009).

[57] M. Fedoruk, M. Meixner, S. Carretero-Palacios, T. Lohmüller, and J. Feldmann, *Nanolithography by Plasmonic Heating and Optical Manipulation of Gold Nanoparticles,* ACS Nano **7**, 7648 (2013).

[58] M. Pelton, J. E. Sader, J. Burgin, M. Liu, P. Guyot-Sionnest, and D. Gosztola, *Damping of acoustic vibrations in gold nanoparticles,* Nat. Nanotechnol. **4**, 492 (2009).